Chinese Physics Letters

LETTER

Hilbert Subspace Imprint: a New Mechanism for Non-Thermalization

Cite as: Hui Yu *et al*. 2026 *Chin. Phys. Lett.* **43** 070701

Recommended Articles

Non-Hermitian Skin Effects in Fragmented Hilbert Spaces of One-Dimensional Fermionic Lattices
Yi-An Wang, and Linhu Li
Chin. Phys. Lett. **42**, 037301 (2025)

Diagnosing Thermalization Dynamics of Non-Hermitian Quantum Systems via GKSL Master Equations
Yiting Mao, Peigeng Zhong, Haiqing Lin, Xiaoqun Wang, and Shijie Hu
Chin. Phys. Lett. **41**, (2024)

Non-reciprocal Synchronization in Thermal Rydberg Ensembles
Yunlong Xue, and Zhengyang Bai
Chin. Phys. Lett. **43**, 010302 (2026)

Some Modified Equations of the Sine-Hilbert Type
Ling-Juan Yan, Ya-Jie Liu, and Xing-Biao Hu
Chin. Phys. Lett. **41**, (2024)

Quantum and Semiclassical Non-Hermitian Dicke Models without Nonreciprocity
Bin Jiang, Yi-Yang Li, Jun-Jie Liu, Chen Wang, and Jian-Hua Jiang
Chin. Phys. Lett. **42**, 120403 (2025)

Machine-Learning Accelerated Discovery of High-Performance Thermal Switch in Two-dimensional Materials Considering High-order Anharmonicity
Jie Sun, Han Meng, Rulei Guo, Long Cheng, Yiheng Shen, and Xiaoliang Zhang
Chin. Phys. Lett. **42**, 110701 (2025)

A series journal of Chinese Physical Society distributed by IOP Publishing

Chinese Physics Letters

Chin. Phys. Lett. **43** 070701 (2026)

LETTER

DOI: 10.1088/0256-307X/43/7/070701
CSTR: 32039.14.0256-307X.43.7.070701

Hilbert Subspace Imprint: a New Mechanism for Non-Thermalization

Hui Yu[1], Jiangping Hu[1,2,*], and Shi-Xin Zhang[1,*]

[1]Beijing National Laboratory for Condensed Matter Physics and Institute of Physics, Chinese Academy of Sciences, Beijing 100910, China
[2]New Cornerstone Science Laboratory, Institute of Physics, Chinese Academy of Sciences, Beijing 100190, China

[*]Corresponding authors. Email: jphu@iphy.ac.cn; shixinzhang@iphy.ac.cn

The search for non-ergodic mechanisms in quantum many-body systems has become a frontier area of research in non-equilibrium physics. In this work, we introduce Hilbert subspace imprint (HSI)—a new mechanism that enables evasion of thermalization, standing as an independent non-ergodic mechanism alongside quantum many-body scars (QMBS) and Hilbert space fragmentation (HSF). HSI manifests when initial states overlap exclusively with a polynomial scaling (with system size) set of eigenstates. We demonstrate this phenomenon through two distinct approaches: weak symmetry breaking and initial state engineering. In the former case, we observe that ferromagnetic states including those with a single spin-flip display non-thermal behavior under weak $U(1)$ breaking, while antiferromagnetic states thermalize. In contrast, the Z_2-symmetric model shows thermalization for both ferromagnetic and antiferromagnetic states. In the latter case, we engineer the initial state prepared by shallow quantum circuits that enhance the overlap with the small target subspace.

Introduction

Thermalization [1,2] in quantum many-body systems refers to the process by which a non-equilibrium system evolves toward a state that can be described by equilibrium statistical mechanics. The eigenstate thermalization hypothesis (ETH) [3–5] provides a framework for understanding thermalization in isolated quantum many-body systems. Specifically, expectation values of observables in eigenstates vary smoothly with energy and match micro-canonical predictions, ensuring that local observables relax to thermal equilibrium values. This explains why most quantum systems equilibrate, despite their underlying unitary dynamics.

While ETH successfully explains thermalization in generic quantum many-body systems, certain mechanisms lead to violations of ETH with persistent non-thermal behavior. One such pathway is quantum integrability [6,7], where an extensive set of conserved quantities prevents thermalization due to exact solvability and insufficient chaotic dynamics with prominent examples [8,9] solvable via the Bethe ansatz [10]. Another violation of ETH arises in many-body localized (MBL) systems [11–16], where strong disorder [17,18] or quasiperiodic potentials [19–21] lead to logarithmic entanglement growth [22–28] and emergent local integrals of motion [29,30]. Another non-thermalization mechanism is prethermalization [31,32] where systems remain in a long-lived metastable state before eventual thermalization. This occurs either through weak integrability-breaking perturbations [33–35] or under strong periodic driving [36–38], where emergent quasi-conserved quantities constrain dynamics over exponentially long timescales.

Beyond these, quantum many-body scars (QMBS) [39–44] typically feature rare, low-entanglement eigenstates [45] embedded within an otherwise thermal spectrum, provides another route to ergodicity breaking. The paradigmatic example is the PXP model [46,47], introduced to describe the Rydberg atom arrays [48] with the nearest-neighbor blockade interactions. Since its discovery, the PXP model has become a cornerstone for understanding QMBS, sparking extensive theoretical and experimental investigations [49–72]. Another mechanism for ergodicity breaking is Hilbert space fragmentation (HSF) [41,73–82], where the Hilbert space dynamically fractures into exponentially many disconnected subsectors known as Krylov subspaces. These subspaces are often related to dynamical constraints and not distinguished by conventional symmetry charges [41]. HSF has been extensively studied in systems with dipole-moment conservation [73,74,83] as well as other systems with constraints [84–89]. Beyond ergodicity breaking, HSF provides a rich platform for novel phenomena including Krylov-restricted thermalization [85,90] and subdiffusive dynamics [91–94].

While previous studies have extensively explored non-thermal dynamics through established mechanisms, a fundamental question remains: do alternative pathways exist to suppress thermalization? Here, we introduce Hilbert subspace imprint (HSI) as a new mechanism for stabilizing non-thermal dynamics. HSI occurs when a short-range entangled initial state has significant overlap with only a polynomially small subset of the system's eigenstates. This framework defines a new route to non-ergodicity distinct from both QMBS and HSF. Unlike QMBS, where the initial state overlaps with a few eigenstates of non-trivial entanglement structure, HSI allows overlap with a polynomially growing number of eigenstates that need not be individually special. On the other hand, it describes a form of initial-state-dependent dynamical confinement, where only a small subset of computational basis states form non-thermal Krylov sectors within the thermal background, which differs from HSF that decomposes the entire Hilbert space into an exponential number of disconnected subspaces. Moreover, the eigenstates comprising the HSI subspace are not required to have low entanglement or special structures like equal energy spacing. The non-ergodicity in HSI is an emergent, collective property of the subspace itself, arising from the fact that a simple initial state has its evolution approximately confined to this small but structurally generic corner of the Hilbert space. This makes HSI a mechanism that can explain non-thermal behavior in systems lacking individually anomalous eigenstates. A schematic comparison of these mechanisms is presented in Fig. 1(a). Exploring how HSI emerge naturally in quantum many-body systems will deepen our understanding of non-thermal phenomena and pave the way for harnessing HSI to engineer long-lived coherent states in experiments.

Received 15 April 2026; accepted 23 May 2026; published 15 July 2026
© 2026 Chinese Physical Society and IOP Publishing Ltd. All rights, including for text and data mining, AI training, and similar technologies, are reserved.

Check for updates

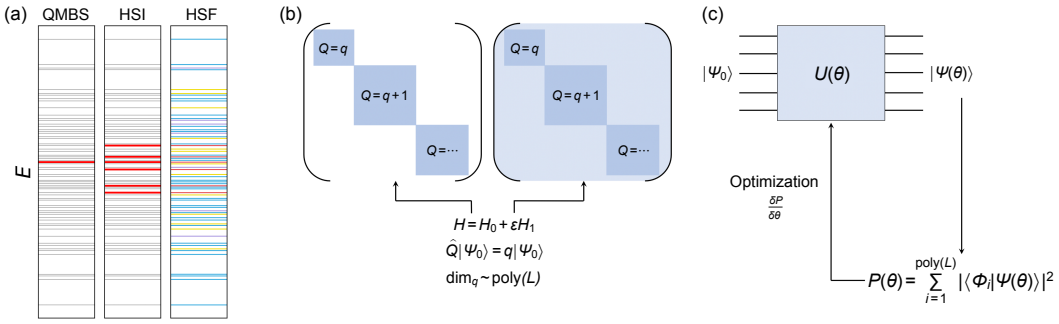

Fig. 1. (a) Displays the energy spectrum for three distinct non-thermal mechanisms. QMBS: The red line marks the scar eigenstate. HSI: Red lines denote a small set of eigenstates restricted to a subspace due to the overlap with certain initial states. HSF: The Hilbert space fractures into disconnected subspaces due to symmetry constraints. Eigenstates of the same color belong to the same subspace except the gray lines for thermal eigenstates. (b) Illustrates weak symmetry breaking mechanism leading to HSI. Here, H_0 is symmetric in terms of symmetry operator $\hat{Q}$, while H_1 breaks the symmetry, indicated by colors outside the blocks. The symmetry breaking strength is tuned by ϵ. The initial state $|\psi_0\rangle$, with symmetry charge q, mainly overlaps with poly(L) eigenstates under weak symmetry breaking. (c) Demonstrates initial state engineering mechanism for HSI. The initial product state is processed through a shallow variational quantum circuit parameterized by θ. The overlap probability between the resulting state $|\psi(\theta)\rangle$ and the target subspace spanned by eigenstates $|\phi_i\rangle$ is iteratively optimized until convergence.

Setup

In this Letter, we demonstrate approximate HSI in which an easily prepared state significantly overlaps with $O(L)$ eigenstates (more than 80% probability weight). The remaining contribution, arising from states outside this subspace, does not grow with time (see Supplementary Material (SM) for derivation). We establish two distinct realization mechanisms for approximate HSI, as illustrated in Figs. 1(b) and 1(c): (1) Weak symmetry breaking. Consider an initial product state $|\psi_0\rangle$ that lives exclusively in one charge sector of dimension poly(L) of a symmetric Hamiltonian H_0, when a weak symmetry-breaking perturbation H_1 is introduced, the eigenstates of the full Hamiltonian $H = H_0 + H_1$ remain adiabatically connected to those of H_0. Consequently, $|\psi_0\rangle$ retains significant overlap with only poly(L) eigenstates of H, leading to desired non-ergodic dynamics. (2) Initial state engineering. The initial state can go beyond the simple product state which is prepared by a shallow-depth parameterized quantum circuit with tunable parameters θ. By optimizing θ, we can obtain the initial state $|\psi(\theta)\rangle$ accessible in experiments of the largest overlap with the target polynomial-sized Hilbert subspace. Both approaches are immediately realizable on current quantum devices, significantly enhancing the experimental accessibility of HSI.

To quantify HSI, we establish a criterion based on the system size scaling of N-the minimum number of eigenstates $\{|E_i\rangle\}$ required to capture 80% of the initial state's weight. The system size dependence of $N(L)$ serves as a quantitative indicator: thermalizing states exhibit characteristic exponential scaling $N \sim e^L$, while non-thermal states follow at most polynomial growth $N \sim \text{poly}(L)$. Moreover, we analyze the time-dependent probability distribution $P_Q(t)$ and entanglement entropy S_a for the dynamics. Here, P_Q at time t is defined as

$$P_Q(t) = \sum_{q=Q} |\langle\psi(t)|\phi_q\rangle|^2, \tag{1}$$

where Q labels the charge sector, $|\psi(t)\rangle$ is the time-evolved state, and $|\phi_q\rangle$ denotes the basis wave function corresponding to charge q. The entanglement entropy (EE) S_a of subsystem a is given by: $S_a = -\text{Tr}(\rho_a \log \rho_a)$, where ρ_a is the reduced density matrix obtained by tracing out all degrees of freedom outside a. Throughout our analysis, we consider the bipartition where subsystem a comprises exactly half of the total system. Together, these quantities offer complementary signatures of thermalization, allowing us to systematically identify initial states with HSI, distinguishing them from thermalizing dynamics.

In our analysis, we examine two initial states: the ferromagnetic (F) state $|000...0\rangle$ and the antiferromagnetic (AF) state $|0101..1\rangle$. Additionally, we consider F state with a single spin flip at the chain center. To track the evolution of charge sector distributions, we numerically simulate the Hamiltonian dynamics through exact diagonalization: $|\psi(t)\rangle = e^{-iHt}|\psi_0\rangle$, where H denotes the target Hamiltonian. All simulations are performed using the TensorCircuit-NG package [95].

Hamiltonian with Weak $U(1)$ Symmetry Breaking

We investigate the Hamiltonian with periodic boundary conditions:

$$\begin{aligned} H_{U1} = &-\sum_{j=1}^{L}\left[\sigma_j^x\sigma_{j+1}^x + \gamma\sigma_j^y\sigma_{j+1}^y + \lambda_1\sigma_j^z\sigma_{j+1}^z\right] \\ &-\lambda_2\sum_{j=1}^{L}\left[\sigma_j^x\sigma_{j+2}^x + \sigma_j^y\sigma_{j+2}^y + \sigma_j^z\sigma_{j+2}^z\right] + h\sum_{j=1}^{L}\sigma_j^z, \end{aligned} \tag{2}$$

where σ_j^α ($\alpha = x,y,z$) are Pauli matrices acting on site j, with $\lambda_1 = 0.2$ and $\lambda_2 = 0.32$ representing the nearest-neighbor and next-nearest-neighbor coupling strengths, respectively. The anisotropy parameter γ breaks the system's $U(1)$ symmetry when $\gamma \neq 1$. The conserved $U(1)$ charge is $\hat{Q} = \sum_{i=1}^{L}\sigma_i^z$. We also include a small longitudinal field $h = 10^{-7}$ to lift degeneracies. The NNN interaction is introduced to make the Hamiltonian non-integrable.

We first examine the system-size scaling of N for the F state at $\gamma = 0.9$. As shown in Fig. 2(a), N remains approximately constant as L increases. For $L = 12$, only a single eigenstate (with more than 90% overlap with the F state) contributes to N. This QMBS state is identified by its anomalous position in the energy spectrum (red dot) and its low half-chain EE, representing a limiting case of HSI. The QMBS nature is manifested in the charge distribution, where the population is predominantly concentrated in the $Q = 12$ sector with minimal leakage to $Q = 8$, as in Fig. 2(c). In contrast, the AF state exhibits thermalization behavior. Figure 2(b) reveals that N grows exponentially with L even under the $U(1)$-symmetric Hamiltonian, a trend confirmed by the linear relationship between N and L on a log-linear scale presented in the SM. This growth accelerates when the symmetry is weakly broken. The distinct thermal character of the AF state is further reflected in its entanglement dynamics [Fig. 2(d)], where the saturated EE reaches values significantly higher than the EE of the F state. Notably, when $1-\gamma$ increases to 0.7 (strong symmetry breaking), the F state also crosses over to thermal behavior. The corresponding time evolution of P_Q for this regime is presented in the SM, where the charge distribution spreads across all symmetry-allowed sectors without preferential occupation.

Now we proceed to investigate the thermal properties of a spin-flipped F state, initialized with a single spin flip at the $L/2$-th site [96]. Under weak symmetry breaking ($\gamma = 0.9$), this state exhibits robust non-thermal behavior, manifested in the polynomial scaling of N with system size shown in Fig. 3(a). Unlike the F state, the spin-flipped case receives contributions from $O(L)$ eigenstates (red markers), combining both QMBS and non-scar volume-law entangled eigenstates. This multi-state involvement represents the generic HSI scenario for non-thermal dynamics, generalizing the QMBS scenario

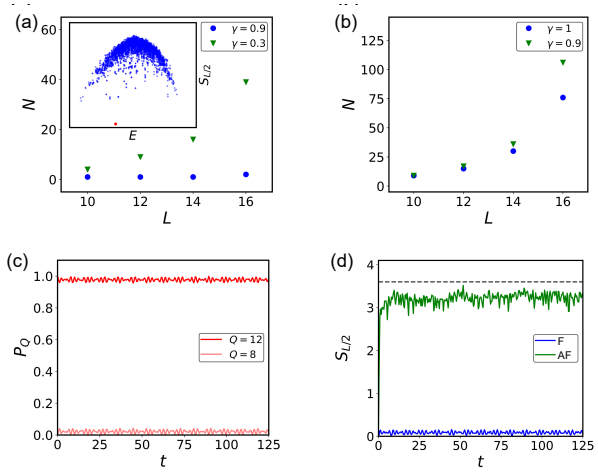

Fig. 2. Static and dynamical properties for H_{U1} from F and AF initial states (QMBS case). The system-size dependence of N for (a) F and (b) AF initial states at various symmetry-breaking strengths γ. The inset displays half-chain entanglement entropy $S_{L/2}$ versus energy E at $L = 12$, with blue dots marking all eigenstates and the red dot highlighting the scar state (>80% overlap with initial states). (c) Presents the charge distribution dynamics $P_Q(t)$ for the F state for $L = 12$ at $\gamma = 0.9$, where negligible-population sectors ($Q = 4, 0, -4, -8, -12$) are omitted. (d) Compares entanglement entropy dynamics between F and AF states for $L = 12$ at $\gamma = 0.9$. The black dotted line indicates the Page value, the expected entanglement entropy for a generic thermalizing state.

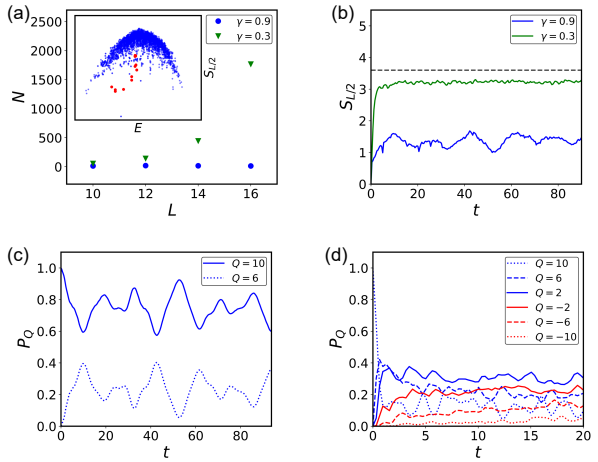

Fig. 3. Static and dynamical properties for H_{U1} from F state with a single spin flip (HSI case). (a) Displays $N(L)$ for the initial spin-flip F state at varying γ. The inset shows the half-chain entanglement entropy versus energy at $L = 12$, with blue dots indicating eigenstates and red dots marking eigenstates contributing to N. (b) Illustrates the half-chain entanglement entropy $S_{L/2}$ dynamics at $\gamma = 0.9, 0.3$ for $L = 12$. The black dotted line denotes the Page value. (c) and (d) Present the charge distribution dynamics $P_Q(t)$ at $\gamma = 0.9, 0.3$ for $L = 12$, omitting $Q = -2, -6, -10$ sectors in (c) due to their negligible populations. All calculations are obtained under H_{U1}.

from the F state case. A clear thermal crossover emerges when increasing the asymmetry to $1 - \gamma = 0.7$, where $N(L)$ transitions from polynomial to exponential scaling. This thermalization is further corroborated by entanglement dynamics in Fig. 3(b). In the SM, we further analyze the behavior of the size dependence of steady state EE: while it remains almost constant in the non-thermal regime, it grows linearly with L in the thermal regime, consistent with volume-law scaling. The charge distribution dynamics in Figs. 3(c) and 3(d) provide additional distinguishing features. When $\gamma = 0.9$, P_Q remains sharply peaked in the $Q = 10$ and $Q = 6$ sectors, confirming the non-thermal character of the state. In contrast, at $\gamma = 0.3$ we observe complete thermalization, with P_Q distributed across all accessible charge

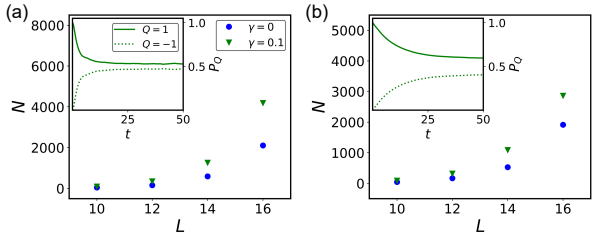

Fig. 4. Thermalization behavior for H_{Z2} model. N versus system size L for the (a) F and (b) AF initial states with different γ values. The insets show the dynamics of charge distributions $P_Q(t)$ for $L = 12$ at $\gamma = 0.1$. All results are averaged over 400 independent realizations.

sectors permitted by the symmetry. The enhanced population in $Q = \pm 2$ sectors is due to their larger Hilbert space dimensionality.

We further investigate the dynamics of F and AF states under weak $U(1)$ symmetry breaking in a disordered Hamiltonian. The F state also exhibits persistent non-thermal dynamics, whereas the AF state undergoes rapid thermalization (see SM).

Hamiltonian with Weak Z_2 Symmetry Breaking

We now study the thermalization properties of F and AF states under a disordered Hamiltonian with explicit breaking of the discrete Z_2 symmetry. The system is described by

$$H_{Z2} = -\sum_{j=1}^{L} \left[\sigma_j^x \sigma_{j+1}^x + \Delta_1 \sigma_j^z \sigma_{j+1}^z + \gamma \sigma_j^x\right] - \sum_{j=1}^{L} h_j \sigma_j^z, \qquad (3)$$

where $\Delta_1 = 0.84$ sets the nearest-neighbor coupling strength. The spatial-dependent fields h_j are sampled uniformly from $[-W, W]$ with $W = 2.4$. The Z_2 symmetry, is generated by the parity operator $\hat{Q} = \prod_{i=1}^{L} \sigma_i^z$, is explicitly broken by the σ^x term with strength γ, as σ^x flips spins. All physical quantities are obtained by averaging over multiple disorder realizations.

Notably, even when the Hamiltonian preserves Z_2 symmetry ($\gamma = 0$), the F initial state exhibits thermalization signatures, evidenced by the exponential scaling of $N(L)$ in Fig. 4(a). This arises from the exponential Hilbert space dimension of the $Q = 1$ sector. Introducing $\gamma > 0$ enhances thermalization, as the new basis state is a superposition of basis in $Q = 1$ and $Q = -1$ sectors. Consequently, the initial states can have nonzero overlap with $Q = -1$ basis states. This fact is further confirmed by computing the time evolution of the sectors $P_{Q=1}$ and $P_{Q=-1}$, as shown in the inset of Fig. 4(a). Similar calculations for the AF state reveal analogous thermalization behavior under the same symmetry-breaking conditions, as reflected in Fig. 4(b).

Initial State Engineering

Recent advances in quantum information processing have enabled high-fidelity state preparation protocols, providing new opportunities to realize and enhance HSI. By implementing a variational quantum circuit [97–101] (see SM for architecture details), we can engineer the target initial state to better confine it within a small Hilbert subspace spanned by these $O(L)$ eigenstates. The circuit comprises N_L layers, each comprising three layers of single-qubit gates followed by one layer of two-qubit gates. We initialize the system in the F state with a single spin flip, as previously described, and train the circuit until the overlap probability with the target eigenstates converges. As revealed in Figs. 5(a) and 5(b), the trained state with $N_L = 5$ achieves 97% overlap weight in the desired subspace. Further increasing N_L to 7 or higher optimizes this overlap to near unity, producing a state with even stronger non-thermal characteristics and nearly perfect HSI. This is further illustrated in Figs. 5(c) and 5(d) through both charge probability distribution and EE dynamics. Unlike the untrained state in Fig. 3(c), the trained state concentrates nearly 100% of its weight in the $Q = 10$ sector while displaying lower EE. This approach offers a

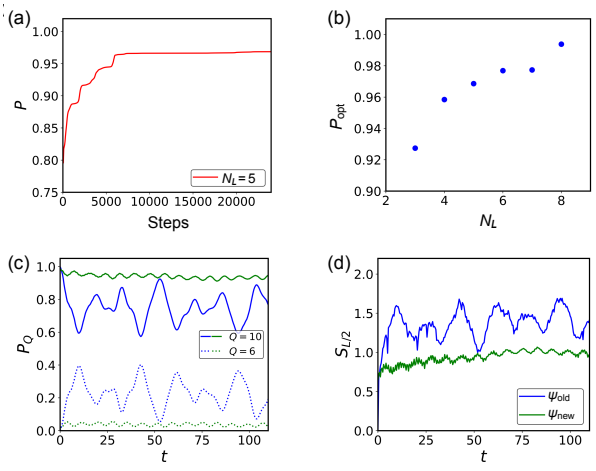

Fig. 5. (a) Tracks the training history of the overlap probability P between the trained state and the target eigenstate subspace for a 5-composite layers quantum circuit acting on an input state of 11 spin-up qubits with a single spin-down at the 6th position. (b) Shows the optimal overlap probability P_{opt} versus increasing the number of circuit layers. Charge dynamics comparison between pre- (blue) and post-optimization (green) states are presented in (c), where negligible-population sectors $Q = 2, -2, -6, -10$ are omitted. (d) Compares the entanglement entropy dynamics between pre- and post-optimization states. All results in (c) and (d) are obtained for H_{U1}.

new perspective on non-ergodicity, moving from Hamiltonian-centric to state-centric with profound implications for preparing and manipulating long-lived states. Moreover, as demonstrated in the SM, with this approach, HSI can be achieved at a stronger symmetry-breaking strength ($\gamma = 0.6$). This confirms that HSI is a generic phenomenon without requiring a small parameter, broadening its applicability and relevance to experimental quantum systems.

Conclusions and Discussions

In this paper, we establish HSI as a distinct mechanism for non-thermalization, alongside QMBS and HSF. We demonstrate HSI through two complementary approaches. First, we show that weak symmetry breaking can induce HSI depending on initial states and the symmetry group. Second, we utilize a constructive, state-centric approach, designing a variational quantum circuit to maximize its overlap with a target non-thermal subspace. We emphasize that HSI is distinct from prethermalization: unlike prethermal states that eventually thermalize, HSI states remain non-ergodic indefinitely, as the leakage weight outside the imprinted subspace is fixed by the initial state and does not grow with time (see SM for the analytical bound). Experimentally, HSI can be directly diagnosed through the charge sector probability distribution P_Q, which has support on only $O(L)$ outcomes and is therefore efficiently accessible via projective measurements on current quantum platforms such as Rydberg atom arrays, trapped ions, and superconducting qubits.

This work opens several avenues for further investigation. A natural extension involves generalizing the framework of weak symmetry breaking to non-Abelian groups, such as $SU(2)$. Furthermore, exploring the relationship between HSI and the quantum Mpemba effect [102–107] promises to yield fundamental insights into the interplay of thermalization and symmetry restoration. Finally, moving beyond the established paradigms of weak symmetry breaking and initial state engineering, an investigation into alternative mechanisms could reveal new strategies for inducing and controlling HSI.

Data Availability

Numerical data for this manuscript are publicly accessible in Ref. [108].

Acknowledgement

We acknowledge helpful discussions with Shuo Liu and Jie Ren. We acknowledge the support by the Ministry of Science and Technology (Grant No. 2022YFA1403900), the National Natural Science Foundation of China (Grant No. 12494594), and the New Cornerstone Investigator Program. HY is also supported by the International Young Scientist Fellowship of Institute of Physics Chinese Academy of Sciences (Grant No. 202407). SXZ acknowledges the support from the Quantum Science and Technology-National Science and Technology Major Project (Grant No. 2024ZD0301700), the National Natural Science Foundation of China (Grant No. 12574546), and the Chinese Academy of Sciences (Grant Nos. XDB1680201 and YSBR-150).

References

[1] Deutsch J M 1991 *Phys. Rev. A* **43** 2046
[2] Rigol M, Dunjko V, and Olshanii M 2008 *Nature* **452** 854
[3] Srednicki M 1994 *Phys. Rev. E* **50** 888
[4] D'Alessio L, Kafri Y, Polkovnikov A, and Rigol M 2016 *Adv. Phys.* **65** 239
[5] Deutsch J M 2018 *Rep. Prog. Phys.* **81** 082001
[6] Olshanetsky M and Perelomov A 1983 *Phys. Rep.* **94** 313
[7] Franchini F 2017 *An Introduction to Integrable Techniques for One-Dimensional Quantum Systems* (Springer Cham) **940**
[8] Baxter R J 1972 *Ann. Phys.* **70** 323
[9] Lieb E H and Liniger W 1963 *Phys. Rev.* **130** 1605
[10] Bethe H 1931 *Z. Phys.* **71** 205
[11] Nandkishore R and Huse D A 2015 *Annu. Rev. Condens. Matter Phys.* **6** 15
[12] Altman E and Vosk R 2015 *Annu. Rev. Condens. Matter Phys.* **6** 383
[13] Abanin D A and Papić Z 2017 *Ann. Phys.* **529** 1700169
[14] Abanin D A, Altman E, Bloch I, and Serbyn M 2019 *Rev. Mod. Phys.* **91** 021001
[15] Alet F and Laflorencie N 2018 *C. R. Phys.* **19** 498
[16] Gunawardana T M and Buča B 2022 *Phys. Rev. B* **106** L161111
[17] Žnidarič M, Prosen T, and Prelovšek P 2008 *Phys. Rev. B* **77** 064426
[18] Pal A and Huse D A 2010 *Phys. Rev. B* **82** 174411
[19] Iyer S, Oganesyan V, Refael G, and Huse D A 2013 *Phys. Rev. B* **87** 134202
[20] Khemani V, Sheng D, and Huse D A 2017 *Phys. Rev. Lett.* **119** 075702
[21] Zhang S X and Yao H 2018 *Phys. Rev. Lett.* **121** 206601
[22] Bardarson J H, Pollmann F, and Moore J E 2012 *Phys. Rev. Lett.* **109** 017202
[23] Deng D L, Li X, Pixley J, Wu Y L, and Das Sarma S 2017 *Phys. Rev. B* **95** 024202
[24] Huang Y, Zhang Y L, and Chen X 2017 *Ann. Phys.* **529** 1600318
[25] Fan R, Zhang P, Shen H, and Zhai H 2017 *Sci. Bull.* **62** 707
[26] Chen X, Zhou T, Huse D A, and Fradkin E 2017 *Ann. Phys.* **529** 1600332
[27] Bañuls M C, Yao N, Choi S, Lukin M D, and Cirac J I 2017 *Phys. Rev. B* **96** 174201
[28] Chen Y Q, Liu S, and Zhang S X 2024 arXiv: 2405.05076 [quant-ph]
[29] Serbyn M, Papić Z, and Abanin D A 2013 *Phys. Rev. Lett.* **111** 127201
[30] Huse D A, Nandkishore R, and Oganesyan V 2014 *Phys. Rev. B* **90** 174202
[31] Berges J, Borsányi S, and Wetterich C 2004 *Phys. Rev. Lett.* **93** 142002
[32] Mori T, Ikeda T N, Kaminishi E, and Ueda M 2018 *J. Phys. B: At. Mol. Opt. Phys.* **51** 112001
[33] Mierzejewski M, Prelovšek P, and Prosen T 2015 *Phys. Rev. Lett.* **114** 140601
[34] Ilievski E, Medenjak M, and Prosen T 2015 *Phys. Rev. Lett.* **115** 120601
[35] Jian S K, Yin S, and Swingle B 2019 *Phys. Rev. Lett.* **123** 170606
[36] Kuwahara T, Mori T, and Saito K 2016 *Ann. Phys.* **367** 96
[37] Mori T, Kuwahara T, and Saito K 2016 *Phys. Rev. Lett.* **116** 120401
[38] Abanin D A, De Roeck W, Ho W W, and Huveneers F 2017 *Phys. Rev. B* **95** 014112
[39] Serbyn M, Abanin D A, and Papić Z 2021 *Nat. Phys.* **17** 675
[40] Chandran A, Iadecola T, Khemani V, and Moessner R 2023 *Annu. Rev. Condens. Matter Phys.* **14** 443

[41] Moudgalya S, Bernevig B A, and Regnault N 2022 *Rep. Prog. Phys.* **85** 086501
[42] Turner C J, Michailidis A A, Abanin D A, Serbyn M, and Papić Z 2018 *Nat. Phys.* **14** 745
[43] Turner C, Michailidis A, Abanin D, Serbyn M, and Papić Z 2018 *Phys. Rev. B* **98** 155134
[44] Choi S, Turner C J, Pichler H, Ho W W, Michailidis A A, Papić Z, Serbyn M, Lukin M D, and Abanin D A 2019 *Phys. Rev. Lett.* **122** 220603
[45] Reference [109] has revealed examples of high-entanglement scars and scarred subspaces spanning a polynomial number of eigenstates. Though the scar state is still highly structured in terms of entanglement with area-law entanglement in some special bi-partitions.
[46] Lesanovsky I and Katsura H 2012 *Phys. Rev. A* **86** 041601
[47] Fendley P, Sengupta K, and Sachdev S 2004 *Phys. Rev. B* **69** 075106
[48] Bernien H, Schwartz S, Keesling A *et al*. 2017 *Nature* **551** 579
[49] Ivanov A N and Motrunich O I 2025 arXiv: 2503.16327 [cond-mat.str-el]
[50] Surace F M, Mazza P P, Giudici G, Lerose A, Gambassi A, and Dalmonte M 2020 *Phys. Rev. X* **10** 021041
[51] Iadecola T, Schecter M, and Xu S 2019 *Phys. Rev. B* **100** 184312
[52] Lin C J and Motrunich O I 2019 *Phys. Rev. Lett.* **122** 173401
[53] Rozon P G, Gullans M J, and Agarwal K 2022 *Phys. Rev. B* **106** 184304
[54] Giudici G, Surace F M, and Pichler H 2024 *Phys. Rev. Lett.* **133** 190404
[55] Windt B and Pichler H 2022 *Phys. Rev. Lett.* **128** 090606
[56] Szołdra T, Sierant P, Lewenstein M, and Zakrzewski J 2022 *Phys. Rev. B* **105** 224205
[57] Ljubotina M, Desaules J Y, Serbyn M, and Papić Z 2023 *Phys. Rev. X* **13** 011033
[58] Desaules J Y, Hudomal A, Banerjee D, Sen A, Papić Z, and Halimeh J C 2023 *Phys. Rev. B* **107** 205112
[59] Desaules J Y, Banerjee D, Hudomal A, Papić Z, Sen A, and Halimeh J C 2023 *Phys. Rev. B* **107** L201105
[60] Kerschbaumer A, Ljubotina M, Serbyn M, and Desaules J Y 2025 *Phys. Rev. Lett.* **134** 160401
[61] Wang H R, Yuan D, Zhang S Y, Wang Z, Deng D L, and Duan L M 2024 *Phys. Rev. Lett.* **132** 150401
[62] Zhang S Y, Yuan D, Iadecola T, Xu S, and Deng D L 2023 *Phys. Rev. Lett.* **131** 020402
[63] Ren J, Liang C, and Fang C 2021 *Phys. Rev. Lett.* **126** 120604
[64] Moudgalya S, Regnault N, and Bernevig B A 2020 *Phys. Rev. B* **102** 085140
[65] Ren J, Hallam A, Ying L, and Papić Z 2025 arXiv: 2504.12383 [cond-mat.quant-gas]
[66] Bull K, Hallam A, Papić Z, and Martin I 2022 *Phys. Rev. Lett.* **129** 140602
[67] Gotta L, Moudgalya S, and Mazza L 2023 *Phys. Rev. Lett.* **131** 190401
[68] Yao Z, Pan L, Liu S, and Zhai H 2022 *Phys. Rev. B* **105** 125123
[69] Ren J, Wang Y P, and Fang C 2024 *Phys. Rev. B* **110** 245101
[70] Ren J, Liang C, and Fang C 2022 *Phys. Rev. Res.* **4** 013155
[71] Shiraishi N and Mori T 2017 *Phys. Rev. Lett.* **119** 030601
[72] Mori T and Shiraishi N 2017 *Phys. Rev. E* **96** 022153
[73] Sala P, Rakovszky T, Verresen R, Knap M, and Pollmann F 2020 *Phys. Rev. X* **10** 011047
[74] Khemani V, Hermele M, and Nandkishore R 2020 *Phys. Rev. B* **101** 174204
[75] Scherg S, Kohlert T, Sala P, Pollmann F, Hebbe Madhusudhana B, Bloch I, and Aidelsburger M 2021 *Nat. Commun.* **12** 4490
[76] Yang Z C, Liu F, Gorshkov A V, and Iadecola T 2020 *Phys. Rev. Lett.* **124** 207602
[77] Herviou L, Bardarson J H, and Regnault N 2021 *Phys. Rev. B* **103** 134207
[78] Hahn D, McClarty P A, and Luitz D J 2021 *SciPost Phys.* **11** 074
[79] Moudgalya S and Motrunich O I 2022 *Phys. Rev. X* **12** 011050
[80] Moudgalya S, Prem A, Nandkishore R, Regnault N, and Bernevig B A 2022 *Memorial Volume for Shoucheng Zhang* (World Scientific) p. 147
[81] Buča B 2022 *Phys. Rev. Lett.* **128** 100601
[82] Jeyaretnam J, Bhore T, Osborne J J, Halimeh J C, and Papić Z 2025 *Commun. Phys.* **8** 172
[83] Pai S, Pretko M, and Nandkishore R M 2019 *Phys. Rev. X* **9** 021003
[84] De Tomasi G, Hetterich D, Sala P, and Pollmann F 2019 *Phys. Rev. B* **100** 214313
[85] Langlett C M and Xu S 2021 *Phys. Rev. B* **103** L220304
[86] Richter J and Pal A 2022 *Phys. Rev. Res.* **4** L012003
[87] Zadnik L and Fagotti M 2021 *SciPost Phys. Core* **4** 010
[88] Read N and Saleur H 2007 *Nucl. Phys. B* **777** 263
[89] Yang F, Magoni M, and Pichler H 2025 arXiv: 2506.10806 [quant-ph]
[90] Schulz M, Hooley C, Moessner R, and Pollmann F 2019 *Phys. Rev. Lett.* **122** 040606
[91] Feldmeier J, Sala P, De Tomasi G, Pollmann F, and Knap M 2020 *Phys. Rev. Lett.* **125** 245303
[92] Morningstar A, Khemani V, and Huse D A 2020 *Phys. Rev. B* **101** 214205
[93] Iaconis J, Vijay S, and Nandkishore R 2019 *Phys. Rev. B* **100** 214301
[94] Iaconis J, Lucas A, and Nandkishore R 2021 *Phys. Rev. E* **103** 022142
[95] Zhang S X, Allcock J, Wan Z Q *et al*. 2023 *Quantum* **7** 912
[96] This state can be understood as a localized wavepacket formed by a superposition of the quasi-Nambu–Goldstone modes identified in Ref. [69]. While a single quasi-Nambu-Goldstone mode is a delocalized momentum state, the localized product state in our case serves as an experimentally accessible proxy to probe the non-thermal dynamics.
[97] Nielsen M A and Chuang I L 2010 *Quantum Computation and Quantum Information* (Cambridge University Press)
[98] Fisher M P, Khemani V, Nahum A, and Vijay S 2023 *Annu. Rev. Condens. Matter Phys.* **14** 335
[99] Bharti K, Cervera-Lierta A, Kyaw T H *et al*. 2022 *Rev. Mod. Phys.* **94** 015004
[100] Cerezo M, Arrasmith A, Babbush R *et al*. 2021 *Nat. Rev. Phys.* **3** 625
[101] Astrakhantsev N, Lin S H, Pollmann F, and Smith A 2023 *Phys. Rev. Res.* **5** 033187
[102] Ares F, Murciano S, and Calabrese P 2023 *Nat. Commun.* **14** 2036
[103] Ares F, Calabrese P, and Murciano S 2025 arXiv: 2502.08087 [cond-mat.stat-mech]
[104] Yu H, Li Z X, and Zhang S X 2025 arXiv: 2501.13459 [quant-ph]
[105] Liu S, Zhang H K, Yin S, and Zhang S X 2024 *Phys. Rev. Lett.* **133** 140405
[106] Liu S, Zhang H K, Yin S, Zhang S X, and Yao H 2024 arXiv: 2408.07750 [cond-mat.dis-nn]
[107] Chang W X, Yin S, Zhang S X, and Li Z X 2024 arXiv: 2409.06547 [cond-mat.str-el]
[108] Yu H, Hu J, and Zhang S X 2026 *Data for Hilbert subspace imprint: a new mechanism for non-thermalization* [Data set]. Zenodo. https://doi.org/10.5281/zenodo.18240945
[109] Langlett C M, Yang Z C, Wildeboer J, Gorshkov A V, Iadecola T, and Xu S 2022 *Phys. Rev. B* **105** L060301